MADRID
inter.noise 2019
June 16 - 19
NOISE CONTROL FOR A BETTER ENVIRONMENT

Investigation of conservative source term interpolation applied to aeroacoustics

Schoder, Stefan[1]
Vienna University of Technology
Getreidemarkt 9, 1060 Vienna, Austria

Freidhager, Clemens[2]
Vienna University of Technology
Getreidemarkt 9, 1060 Vienna, Austria

Kaltenbacher, Manfred[3]
Vienna University of Technology
Getreidemarkt 9, 1060 Vienna, Austria

ABSTRACT

In low Mach number aeroacoustics, the well known disparity of length scales makes it possible to apply well suited hybrid simulation models using different meshes for flow and acoustics, which leads to a powerful computational procedure. In general, hybrid aeroacoustic methods seek for robust and conservative mesh to mesh transformation of the aeroacoustic sources while high computational efficiency is ensured. We investigate the accuracy of a standard conservative interpolation scheme compared to the more accurate cut-volume-cell approach and their application to the computation of rotating systems, namely an axial fan. The capability and the robustness of the cut-volume-cell interpolation in a hybrid workflow on different meshes are investigated by a grid convergence study.

Keywords: Noise, Environment, Annoyance
I-INCE Classification of Subject Number: 30
(see http://i-ince.org/files/data/classification.pdf)

1. INTRODUCTION

In computational aeroacoustics (CAA) hybrid schemes are used to separate the flow from the acoustic computation employing aeroacoustic analogies [1, 2]. Accordingly, for

[1]stefan.schoder@tuwien.ac.at
[2]clemens.freidhager@tuwien.ac.at
[3]manfred.kaltenbacher@tuwien.ac.at

each physical field optimized computational grids can be used achieving highest accuracy. Anyhow, this implies that the flow and the acoustic grid could be quite diverse and consequently an accurate data transfer from the flow to the acoustic grid is essential to obtain reasonable CAA results. Therefore, several interpolation strategies can be applied, such as low complexity nearest neighbor interpolation or highly involved volume intersections between the two grids. Based on the first application of the cell volume weight interpolation [3], the acoustic effects of the cut-volume-cell approach compared to the limited standard approach are studied [4].

2. METHODOLOGY

2.2.1. Perturbed convective wave equation

To derive the computationally efficient perturbed convective wave equation (PCWE), an acoustic/viscous splitting alike [5] is conducted and an Arbitrary-Eulerian (ALE) description for the operators

$$\frac{D}{Dt} = \frac{\partial}{\partial t} + (\overline{\boldsymbol{v}} - \boldsymbol{v}_\mathrm{r}) \cdot \nabla \,, \tag{1}$$

is introduced. Here, $\overline{\boldsymbol{v}}$ identifies the mean velocity of the flow field and $\boldsymbol{v}_\mathrm{r}$ the relative velocity of the grid. Based on the acoustic perturbation equations [6], we obtain the PCWE for rotating systems [3]

$$\frac{1}{c^2}\,\frac{D^2\psi^\mathrm{a}}{Dt^2} - \Delta\psi^\mathrm{a} = -\frac{1}{\bar{\rho}c^2}\,\frac{Dp^\mathrm{ic}}{Dt}\,, \tag{2}$$

where c denotes the speed of sound, $\bar{\rho}$ the mean density of the flow field and p^ic the incompressible part of the pressure. Using this formulation decreases the number of unknowns (acoustic pressure p^a and particle velocity $\boldsymbol{v}^\mathrm{a}$) to only a scalar unknown, the acoustic velocity potential ψ^a with $\nabla\psi^\mathrm{a} = \boldsymbol{v}^\mathrm{a}$. Based on the PCWE, we verify the source term interpolation of aeroacoustic sources for moving and non-moving meshes.

2.2.2. Source term interpolation

The standard interpolation conserves the energy globally but approximates the local energy conservation of the finite element right hand side by

$$\int_{E^\mathrm{a}} N_i^\mathrm{a}(\boldsymbol{\xi}) f^\mathrm{a} \mathrm{d}\xi = \sum_{\mathrm{k}\in\mathrm{M^f}} \mathrm{N_i^a}(\boldsymbol{\xi}_{\mathrm{E_k^f}})\mathrm{F_k^f}\,, \tag{3}$$

where E_k^f denotes the cell of the flow grid, $\boldsymbol{\xi}_{E_k^\mathrm{f}}$ the local coordinate, M^f the number of flow cells, and the subscript i the node number on the CAA grid. The standard approach includes all nodal loads F_k^f (see Fig. 1a) of the flow cells with nodes inside the respective acoustic finite element E^a. The nodal loads on the CFD mesh are assembled in terms of the finite element method by

$$F_k^\mathrm{f} = \bigwedge_{l\to k} \int_{E_l^\mathrm{f}} N_l^\mathrm{f}(\boldsymbol{\xi}) f^\mathrm{f}(\boldsymbol{\xi}) \mathrm{d}\xi \,. \tag{4}$$

However, we may reduce the computational complexity for fine flow grids by simplifying the integration over the source volume to a first order volume weighting

$$F_k^{\mathrm{f}} = \bigwedge_{l \to k} V_{E_l^{\mathrm{f}}} f_l^{\mathrm{f}}(\boldsymbol{\xi}_{E_l^{\mathrm{f}}}) \,. \tag{5}$$

Finally, the nodal loads F_k^{f} are interpolated to the nodes of the acoustic mesh using finite element basis functions N^{a_i} [4].

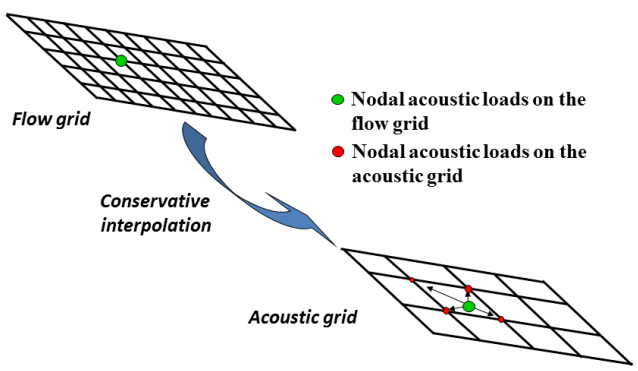

(a) Workflow of the conservative standard interpolation.

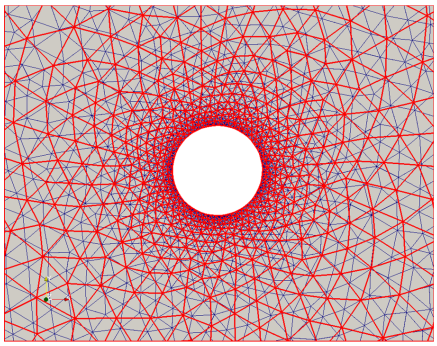

(b) CFD grid (red) and CAA grid (blue).

Figure 1: Standard approach for conservative interpolation and general mesh sizes of flow and acoustic grid.

As long as the flow grid is much finer than the acoustic grid, this standard approach delivers correct results. The discretization density of flow computations diversifies from fine meshes at the boundaries to coarse meshes at regions without flow gradients. However, the discretization of the CAA mesh is supposed to be steady to properly transport waves. Consequently, hybrid aeroacoustic workflows have to be able to handle regions where the density of the flow grid is larger than the density of the acoustic mesh (see Fig. 1b). In cases like this, the stated standard approach does not deliver accurate results because it neglects part of the contributions weighted by the volume. Contrary to the standard interpolation, the cut-volume-cell approach takes for each acoustic volume element E_l^{a} the set of flow cells E^{f} that intersect with the particular acoustic volume element

$$E_l^{\mathrm{f}\cap\mathrm{a}} = E_l^{\mathrm{a}} \cap E^{\mathrm{f}} \tag{6}$$

into account. Thus, this exigent approach conserves the energy globally as well as locally for varying mesh sizes of both the flow and the acoustic grid. The finite element right hand side is computed with

$$\int_{E^{\mathrm{a}}} N_i^{\mathrm{a}}(\boldsymbol{\xi}) f^{\mathrm{a}} \mathrm{d}\xi = \sum_{\mathrm{k}\in\mathrm{M}^{\mathrm{f}\cap\mathrm{a}}} \mathrm{N}^{\mathrm{a}_i}(\boldsymbol{\xi}_{\mathrm{k}}) \mathrm{F}_{\mathrm{k}}^{\mathrm{f}\cap\mathrm{a}} \,, \tag{7}$$

and based on the intersecting cells, the nodal loads $F_k^{\mathrm{f}\cap\mathrm{a}}$ are volume-weighted by

$$F_k^{\mathrm{f}\cap\mathrm{a}} = \bigwedge_{l \to k} \int_{E_l^{\mathrm{f}\cap\mathrm{a}}} N_l^{\mathrm{f}}(\boldsymbol{\xi}) f^{\mathrm{f}}(\boldsymbol{\xi}) \mathrm{d}\xi \,. \tag{8}$$

With the assumption that the aeroacoustic source term is constant for a fluid cell, the integral simplifies to a multiplication of the intersection volume $V_c \multimap V_{E_l^{f\cap a}}$ with the source density f_l^f at the volumetric centroid $\boldsymbol{x}_c \multimap \boldsymbol{\xi}_{E_l^{f\cap a}}$ of the intersection polyhedron

$$F_k^{f\cap a} = \bigwedge_{l\to k} V_{E_l^{f\cap a}} f_l^f(\boldsymbol{\xi}_{E_l^{f\cap a}})\,. \tag{9}$$

The workflow of the algorithm is depicted in Fig. 2. This approach makes it possible to accurately treat the stated problem of an acoustic grid that is finer than the flow grid possible.

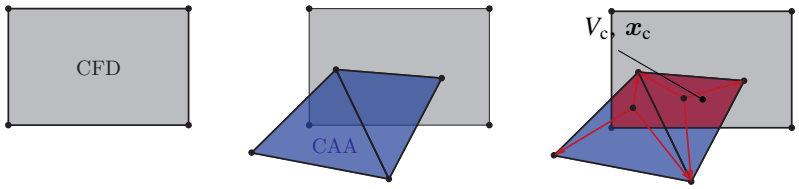

Figure 2: Necessary steps for the interpolation based on the cut-volume-cell approach.

3. RESULTS

The stated approach is now used for the acoustic simulation of a fan (see Fig. 3a) that was already used for investigations in [7]. The fan consists of 9 plates, has a diameter of 0.5 m, is operated at 1500 rpm with a volume flow of 1.3 m^3/s, and is mounted together with the motor into a funnel. A detached eddy CFD simulation was used to obtain the necessary incompressible fluid pressure for computing the source terms with Equation 2. The obtained source terms were first assembled onto the flow grid and in a next step interpolated to the acoustic grid (see Fig. 3b) by using the stated cut-volume-cell interpolation approach. Marked in yellow is the rotating region including the fan, in which the main acoustic source terms emerge. The green region is a stationary propagation region and the red domain marks a perfectly matched layer (PML) to take the free radiation condition into account. The surfaces of the nozzle, duct, strut, driving shaft, and motor are modeled as acoustically hard walls.

In a next step, after the source terms were interpolated to the CAA grid, the acoustic computation was done with our in-house code CFS++ [8]. Following, the resulting power spectral densities (PSD) of the two different simulations using the standard as well as the cut-volume-cell method are compared (see Fig. 4).

Measurements with a measurement time of 30 s and with a measurement time of 0.1 s are depicted in black and gray. Especially the measurement time of 0.1 s is close to the simulation time of 0.08 s. The results of both simulations have a radical drop at a frequency of 6 kHz, because the mesh resolution in the propagation domain becomes too coarse for acoustic wave lengths in this frequency range. The result of the simulation using the standard approach is shown in red. Clearly, it over-predicts the PSD for the entire frequency range and is not adequate for cases with complex geometry and distorted grid cells of varying sizes. However, the result of the cut-volume-cell interpolation, depicted as a blue line, is in good agreement with the performed

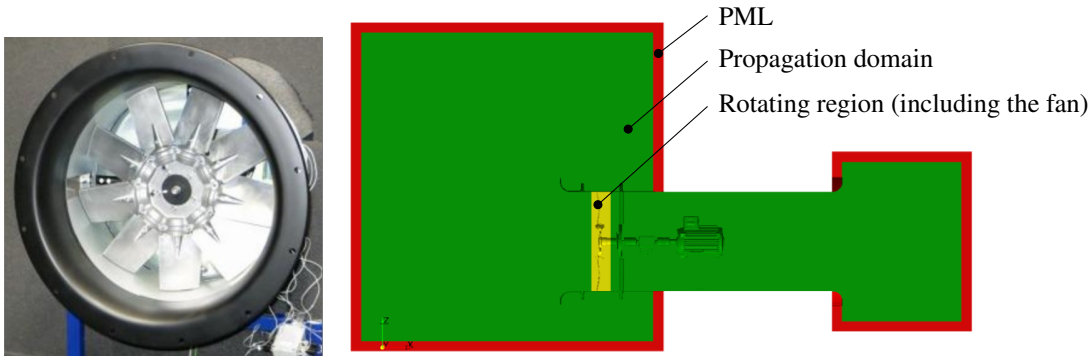

(a) Geometry of the investigated fan. *(b) Geometry of the acoustic domain with the rotating region in yellow.*

Figure 3: Investigated fan.

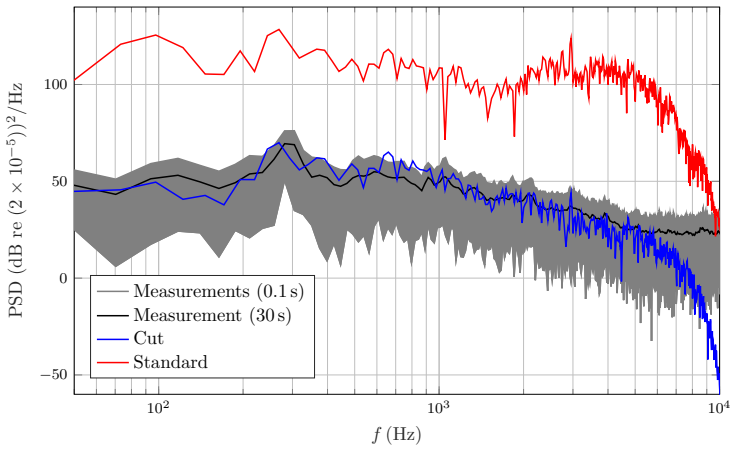

Figure 4: Comparison of the PSD of measurements and the PSD of simulations using the standard and the cut-volume-cell interpolation algorithm, respectively.

measurement. Consequently, for the application on complex geometries this approach delivers the robustness that is required.

Grid convergence study using the cut-volume-cell interpolation

Based on the knowledge that the presented cut-volume-cell interpolation outperforms the standard procedure, the influence of the CAA discretization resolution is investigated. Therefore, the same setup as for the CFD simulation was used to interpolate the acoustic source term to four different grids in the rotating region. All of those grids are tetrahedral and have varying grid densities. The specifications of the four different meshes are shown in Tab. 1, with mesh 1 being the finest and mesh 4 the coarsest grid. Each grid of the rotating region is depicted in Fig. 5a, with the meshes getting coarser from left to right. At least on element has to be used in the tip gap to properly represent the topology. The elements in the tip gap dominate the number of elements for coarse meshes and consequently limit the possible minimal number of elements.

The PSD computed with the four different rotating meshes using the cut-volume-cell approach, as well as the PSD of the corresponding measurements as presented before are shown in Fig. 5b. The dominant peak at a frequency of 300 Hz is a result of the interaction of the tip gap flow and the blade passing frequency. It should be observed that those two

	Total elements	Total nodes	Max. element size in mm
Mesh 1	7690908	1322937	7
Mesh 2	1021697	181186	12
Mesh 3	555562	96535	18
Mesh 4	337013	58708	24

Table 1: Different meshes used in the rotation region to investigate the cut-volume-cell interpolation.

frequencies are not alike, but due to the frequency resolution used in this example they merge to one peak. The colored lines are the results of the numerical simulations using the different meshes. For the low frequency range, each numerical simulation under-predicts the PSD, which might be because of the short numerical simulation time. However, the peak corresponding to the tip gap flow and to the passing of the blades is well represented in frequency and amplitude. In the higher frequency range up to 6 kHz the trend is in good agreement with the measurements depicted in gray and black. At frequencies above 6 kHz the same drop as discussed before can be seen. Up to a frequency of 1 kHz all simulations deliver nearly identical results. The discrepancies between the four computed simulations, especially at high frequencies, are assumed to have their origin in the different grid densities of the source region, where the coarsest mesh meets its limitations to resolve the geometric shape of the source terms. The computed numerical results verify the robustness of the cut-volume-cell interpolation algorithm.

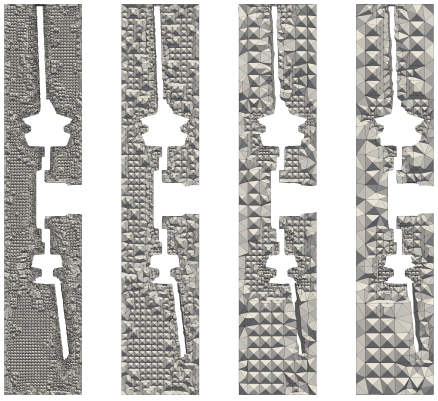

(a) Different meshes used for the computation.

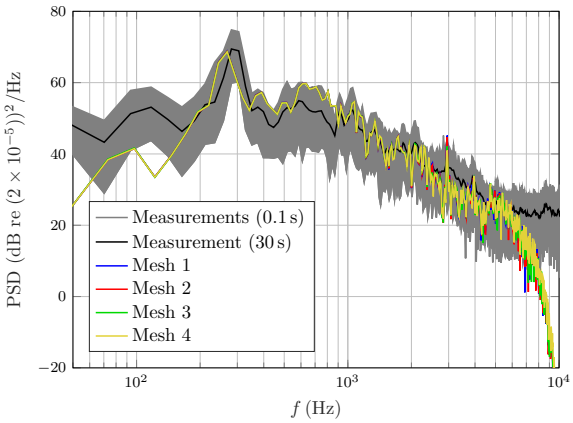

(b) Acoustic power spectral density for different discretizations.

Figure 5: Comparison of different discretizations (from 1 the finest to 4 the coarsest).

4. CONCLUSIONS

In this paper, we presented an approach for the conservative interpolation of source terms in a hybrid acoustic workflow. The proposed cut-volume-cell method considers for each acoustic volume element the intersecting flow cells. Hence, the basis to interpolate source terms, calculated on the CFD grid, to the CAA mesh was created. Consequently, this approach improves robustness for meshes with skewed cells and varying cell sizes, especially when the CAA mesh density becomes higher than the

CFD mesh density. Investigating the aeroacoustic simulations of an axial fan showed that the standard interpolation procedure massively over-predicted the acoustic PSD. However, the presented cut-volume-cell interpolation approach created results that were in good agreement with measurements. In a last step, the robustness of the presented cut-volume-cell interpolation was investigated using different grids in the rotating region. Thus, the results of the finest grid, which only had 4.4 % of the elements of the coarsest grid, were almost identical to the simulation done with the coarsest mesh.

5. REFERENCES

[1] DG Crighton. Computational aeroacoustics for low mach number flows. In *Computational aeroacoustics*, pages 50–68. Springer, 1993.

[2] C. Wagner, T. Hüttl, and P. Sagaut, editors. *Large-Eddy Simulation for Acoustics*. Cambridge University Press, 2007.

[3] M. Kaltenbacher. *Computational Acoustics*. CISM International Centre for Mechanical Sciences. Springer International Publishing, 2017.

[4] M Kaltenbacher, M Escobar, S Becker, and I Ali. Numerical simulation of flow-induced noise using les/sas and lighthill's acoustic analogy. *International journal for numerical methods in fluids*, 63(9):1103–1122, 2010.

[5] JC Hardin and DS Pope. An acoustic/viscous splitting technique for computational aeroacoustics. *Theoretical and Computational Fluid Dynamics*, 6(5-6):323–340, 1994.

[6] Roland Ewert and Wolfgang Schröder. Acoustic perturbation equations based on flow decomposition via source filtering. *Journal of Computational Physics*, 188(2):365–398, 2003.

[7] Manfred Kaltenbacher, Andreas Hüppe, Jens Grabinger, and Barbara Wohlmuth. Modeling and finite element formulation for acoustic problems including rotating domains. *AIAA Journal*, pages 3768–3777, 2016.

[8] Manfred Kaltenbacher. *Numerical simulation of mechatronic sensors and actuators: finite elements for computational multiphysics*. Springer, 2015.